Supporting Information

High yield selective electrochemical conversion of N₂ to NH₃ via morphology controlled silver phosphate under ambient conditions

Divyani Gupta,[a] Alankar Kafle,[a] Sukhjot Kaur [a] Prajna Parimita Mohanty,[b,c] Tisita Das,[c] Sudip Chakraborty,[c] Rajeev Ahuja,[b,d] Tharamani C. Nagaiah[a]*

[a] Department of Chemistry, [b] Department of Physics, Indian Institute of Technology Ropar, Rupnagar, Punjab 140001, India.
[c] Materials Theory for Energy Scavenging (MATES) Lab, Harish-Chandra Research Institute (HRI) Allahabad, HBNI, Chhatnag Road, Jhunsi, Prayagraj (Allahabad) 211019, India
[d] Condensed Matter Theory Group, Department of Physics and Astronomy, Uppsala University, Uppsala, SE-75120, Sweden

*Corresponding author. E-mail address: tharamani@iitrpr.ac.in

Chemicals and reagents used

The chemicals for synthesis *i.e.* silver nitrate (AgNO₃; ≥ 99.8 %,) from Chemlab, trisodium citrate (Na₃C₆H₅O₇; 99 %,) from Reachem, sodium hydroxide (NaOH; 98 %,) from Merck and sodium dihydrogen orthophosphate (NaH₂PO₄; 98 %,) were procured from Alfa Aesar, which are of analytical grade and used without further purification. For quantification of products formed, ammonium chloride (NH₄Cl, 99 %), salicylic acid (C₇H₆O₃, 99.5 %), sodium nitroprusside (C₅FeN₆Na₂O, 99 %), para-dimethylaminobenzaldehyde (p-C₉H₁₁NO, 99 %), sodium nitrate (NaNO₃, 99 %), sodium nitrite (NaNO₂, 98 %), sulphanilamide (C₆H₈N₂O₂S, 99 %), N-(1-Napthyl) ethylenediamine dihydrocholoride (C₁₂H₁₄N₂, 99 %), mercuric (II) iodide (HgI₂), sodium potassium tartrate (C₄H₄O₆KNa·4H₂O), hydrazine monohydrate (N₂H₄.H₂O, 99

%), sodium hypochlorite solution (NaClO, 4-6 %) and hydrogen peroxide solution (H_2O_2, 5 %) were purchased from Loba chemie. $^{15}NH_4Cl$ (99%) was purchased from Cambridge isotope laboratories for isotope labeling measurements. All solutions were prepared using deionized water obtained from Millipore system (15 MΩ). All the analytical grade reagents used in this study such as potassium hydroxide (KOH, 85 %), sodium hydroxide (NaOH), hydrochloric acid (HCl; 37 %) and ethanol (C_2H_5OH; 99 %) were purchased from Loba chemie and Merck respectively and were used as such without further purification and. Nafion N117 membrane fitted in H-cell setup was bought from DuPont. High purity $^{14}N_2$ (99.999%), $^{15}N_2$ (99%) and Ar gas (99.999%) cylinders were purchased from Sigma. All the chemicals and reagents used in this study were of analytical grade and used as such without purification and the deionized water was obtained from Millipore system (>14 MΩ cm^{-1}).

Material characterization

The physical characterizations of synthesized silver phosphate composites were investigated using powder X-ray diffraction (PXRD) measurements in the 2θ range from 5 to 80 degree using PANalytical's X'Pert Pro MPD wherein the X-ray source was Cu Kα radiation. The morphology of each variants was analysed using scanning electron microscopy (FE-SEM, Hitachi, Japan, SU8010). The elemental composition was analysed using energy dispersive X-ray spectroscopic measurements (EDS, Oxford, INCAx-act, 51-ADD0013). Further, silver, phosphorus and oxygen in the matrix was confirmed by performing X-ray photoelectron spectroscopy (XPS, PHI Versa Probe II Spectrometer) working at 15 kV under an ultrahigh vacuum (UHV; 7×10-10 mbar) using Al Kα monochromatic radiation (*hv* = 1486.6 eV). The measurements were performed in fixed transmission mode with a pass energy of 376 eV to obtain Ag 3d, P 2p and O 1s spectra. The obtained spectra were calibrated with respect to C

1s. UV-Visible spectroscopic measurements were performed using SEC2000-DH spectrophotometer. NMR spectra were recorded using a JEOL JNM-ECS 400 Hz spectrometer at ambient probe temperatures and referenced as follows: 1H: residual internal CHCl$_3$ 7.26 ppm; DMSO-d$_6$ 2.50 ppm by applying water suppression.

Quantification of Ammonia[1]

Indophenol blue method: After electrochemical reduction reaction, the amount of ammonia was quantified UV-Visible spectrophotometrically by Indophenol blue method. In detail, in the electrolyte taken after the reduction 2 mL of solution containing 5% salicylic acid and 5% sodium citrate in 1M KOH followed by 1 mL of 0.05 M NaClO and 0.2 mL of 1% C$_5$FeN$_6$Na$_2$O·2H$_2$O were added into the above solution was added and kept standing at room temperature for 2 h and finally the UV-Vis absorption spectrum was measured at a wavelength of 655 nm. The calibration concentration–absorbance curve was generated by using standard NH$_4$Cl solution with known NH$_4^+$ concentrations of 0.1, 0.2, 0.4, 0.8, and 1.0 µg mL^{-1} from which the concentration of ammonia was determined. The rate of ammonia formation was determined according to

$$Yield\ rate(\mu g\ mg^{-1}\ h^{-1}) = \frac{V \times C_{NH_3}}{t \times m_{cat.}}$$

Here, C$_{NH3}$ is the measured NH$_3$ concentration, V the volume of electrolyte, *t* the time of the reduction reaction and m$_{cat}$ is the mass of the catalyst loaded onto GCE.

Similarly, its Faradaic efficiency (F.E.) was calculated as

$$F.E.(\%) = \frac{3 \times F \times V \times C_{NH3}}{17 \times Q}$$

Where F is the Faraday constant and Q is the total amount of charge passed through the electrodes during the electrolysis.[2]

Nessler's reagent method [1]: For validation of NH_3 quantified by Indophenol blue method, Nessler's test was also performed. At first, Nessler's reagent was prepared by adding 2.5 g of mercuric iodide into 5 mL aq. solution of potassium iodide (2 g in 5 mL deionized water) and making final solution of 20 mL by diluting with deionized water. 4 g of NaOH was then added to the above solution and labelled as Nessler's reagent. Briefly, 5 mL of electrolyte solution was collected after e-NRR to which 0.25 mL of sodium potassium tartrate (500 g L^{-1}) and 0.25 mL of Nessler's reagent was added. The above solution mixture was kept undisturbed for 10 minutes followed by UV-Vis. absorption measurement at λ=420 nm. The calibration concentration–absorbance curve was generated by using standard NH_4Cl solution with known NH_4^+ concentrations of 0.1, 0.2, 0.4, 0.8, and 1.0 µg mL^{-1} in a similar way.

Quantification of hydrazine[3]

Watt-Chrisp method: The amount of hydrazine formed during the electrolysis was determined UV-Visible spectrophotometrically by Watt and Chrisp method in which a mixture of p-$C_9H_{11}NO$ (0.4 g), HCl (concentrated, 2 mL) and C_2H_5OH (20 mL) was used as colouring reagent. After electrolysis, 2 mL of electrolyte from cathodic chamber was taken out and 2 mL of colouring solution was added on it. The analyte was kept for 20 minutes and finally the absorbance of the resulting solution was measured at 455 nm. In order to determine the concentration a calibration curve was used which was generated by using standard hydrazine solution with known N_2H_4 concentrations of 0.1,0.2, 0.4, 0.8 and 1.0 µg mL^{-1} in 0.1 M KOH.

Isotope labelling experiments[4]

The isotope labelling experiment was performed by taking $^{15}N_2$ (Sigma-Aldrich 99 atom% ^{15}N) as the feeding gas. The $^{15}N_2$ gas was passed through alkaline $KMnO_4$ followed by dilute H_2SO_4 solution before purging to cell and a fixed amount of gas (25 mL gas in the interval of the 15

minutes) was supplied during the electrolysis at 0 V vs. RHE for 2 h. After electrolysis 25 ml of the electrolyte was taken out and mixed with 1M HCl and then concentrated to 1 mL.

The produced ammonia was confirmed and quantified by using ^{1}H nuclear magnetic resonance measurements (^{1}H NMR) with water suppression method. A single pulse sequence was applied during the relaxation delay of 1 s with a total number of 8000 transient scans and an acquisition time of 2.18 s. Out of the concentrated electrolyte sample, 0.7 ml of the resulting liquid was taken and 0.2 ml of DMSO- d6 was added as an internal standard to achieve sufficient lock signal and 0.125 mL of maleic acid was added for quantification purpose. All other samples ($^{14}N_2$ and Ar saturated) were tested in the similar manner. Calibration curves were extracted for different concentrations of standard $^{14}NH_4Cl$ and $^{15}NH_4Cl$ solutions ranging between 1 to 3 ppm with reference to maleic acid as a standard with a total number of 1024 scans.

Also, the quantification was executed by means of liquid chromatography-mass spectroscopy (LC-MS) technique by following the reported procedure.[5] Briefly 150 µL of phenol solution was mixed with 30 µL of sodium hypochlorite and sodium nitroprusside each. The above solution mixture was then added into 1.5 mL of the NH_4^+ containing standard and sample solution to generate Indophenol blue. After which 15 µL of 10 M HCl was added in order to convert the complex into Indophenol red, which was then extracted by addition of ethyl acetate (1.5 mL) from organic layer. The organic layer was separated from aqueous layer and ethyl acetate was completely evaporated, thereafter the indophenol red was re-dissolved in methanol for LC-MS.
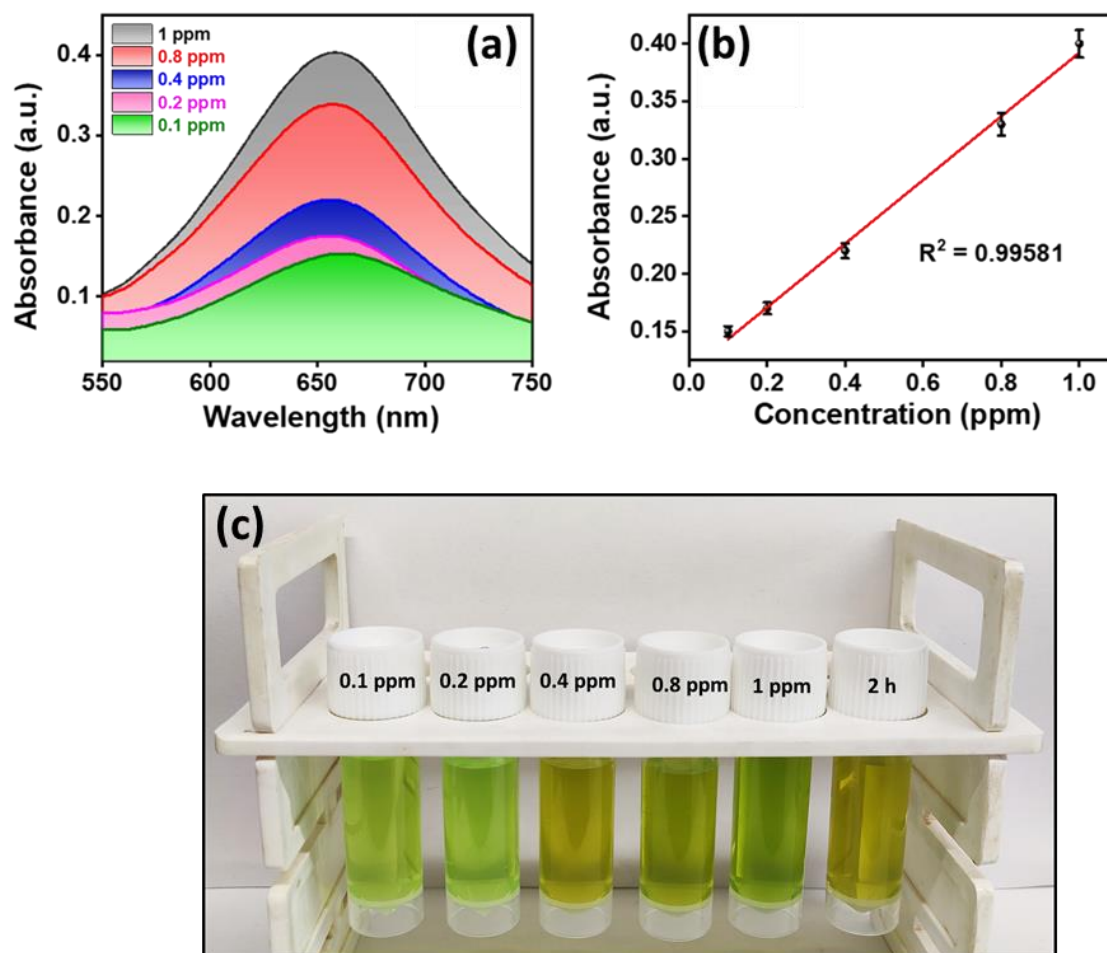
Fig. S1 (a) UV-vis spectrum and (b) calibration curve obtained from known concentrations of standard solution of NH_3 using Indophenol blue method. (c) Images of standard solutions of NH_4^+ with varying concentrations and electrolyte sample collected after 2 h of electrolysis by Ag_3PO_4 (2 h) at 0 V showing colour development during Indophenol blue method.
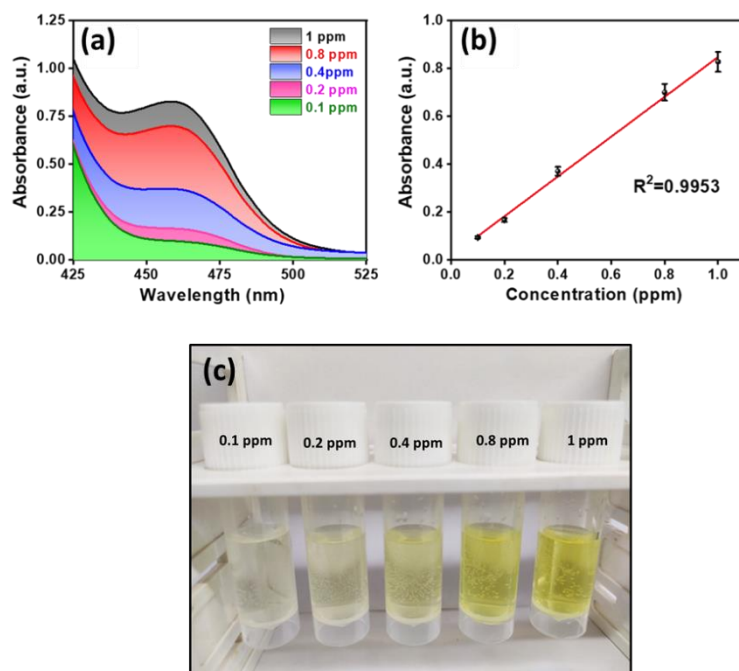
Fig. S2 (a) UV-vis spectra of standard N_2H_4 solutions by Watt and Chrisp method (b) corresponding calibration curve. (c) Images of standard N_2H_4 solutions showing colour development during Watt-Chrisp quantification method.
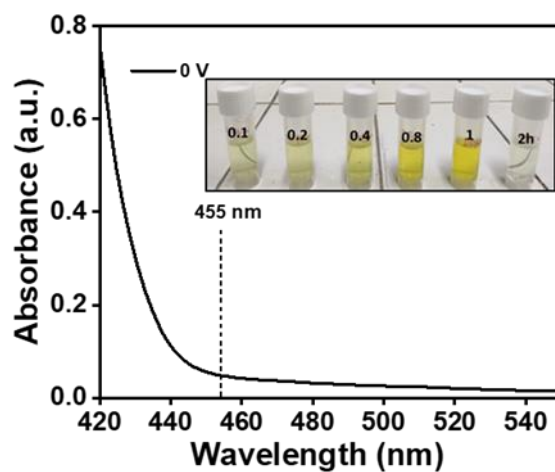

Fig. S3 UV-vis spectrum of electrolyte sample collected [Ag_3PO_4 (2 h)] after 2 h chronoamperometry at 0 V *vs.* RHE for hydrazine determination.
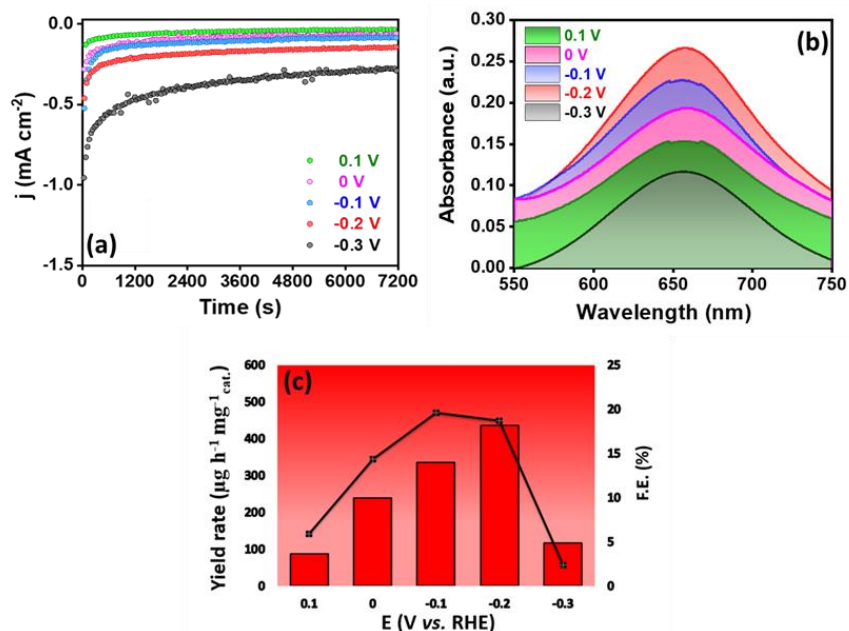
Fig. S4A (a) Chronoamperometric curves obtained at different potentials in N_2 saturated 0.1 M KOH, (b) respective UV-Vis. absorption curves after quantification by Indophenol blue method and (c) Bar graph representing F.E. and NH_3 production yield rate for Ag_3PO_4 (4 h).
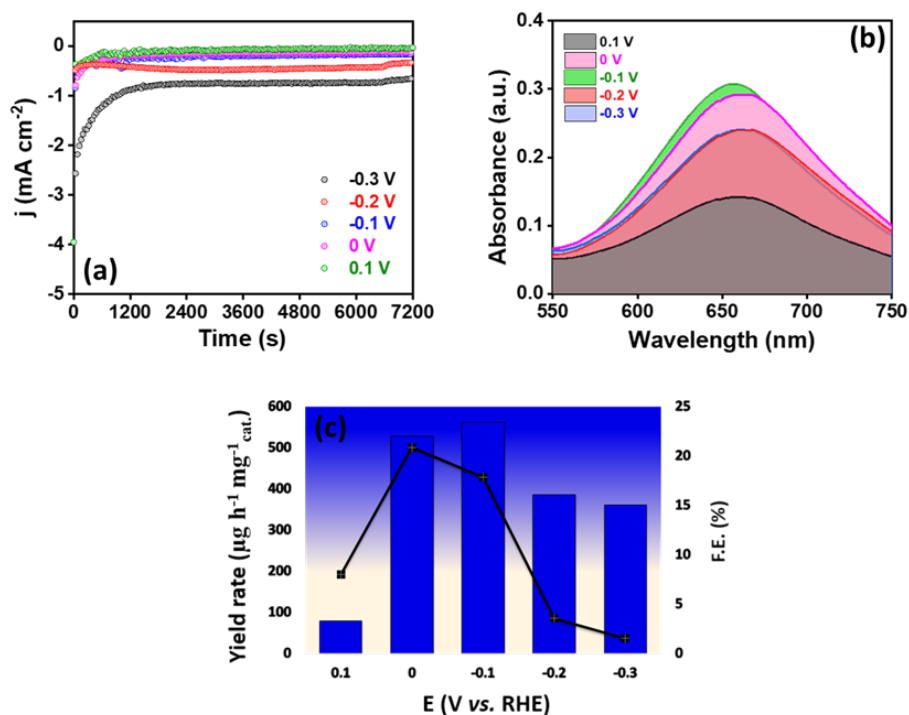

Fig. S4B (a) Chronoamperometric curves obtained after 2 h of electrolysis under N_2 saturated electrolyte, (b) corresponding UV-Vis. absorption curves obtained after quantification and **(c)** Bar diagram screening F.E. and NH_3 production yield rate for Ag_3PO_4 (6 h).
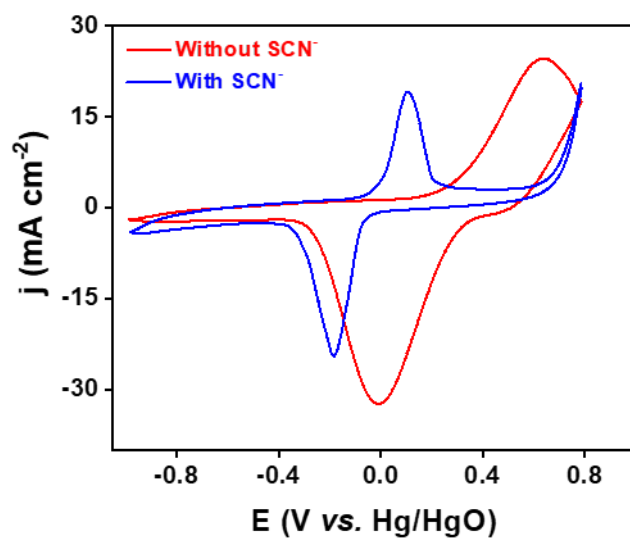
Figure S5A. Cyclic voltammograms acquired for Ag_3PO_4 (2 h) catalyst coated GCE in presence and absence of SCN^- ions.
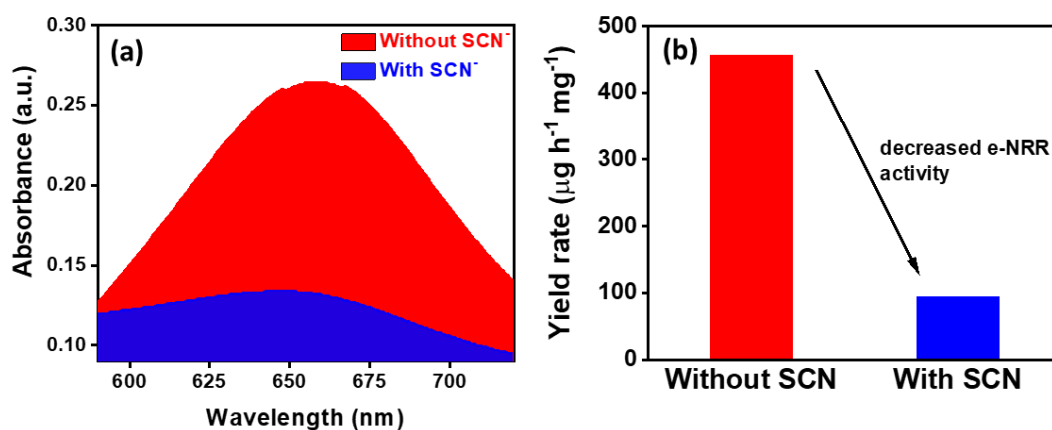

Figure S5B. (a) UV-Vis. absorbance curves obtained by quantification of samples collected after e-NRR by Ag_3PO_4 (2 h) in absence and presence of SCN^-, and (b) Bar diagram comparison of NH_3 yield rate calculated after NRR control experiments in presence and absence of SCN^- ions by Ag_3PO_4 catalyst.

TOF calculations for Ag₃PO₄ (2 h) catalyst during e-NRR:

$$\text{Turnover frequency (TOF)} = \frac{\text{Turnover number (TON)}}{\text{Time (h)}}$$

$$\text{Turnover number (TON)} = \frac{NH_3 \text{yield (mg)}}{\text{Catalyst loading (mg)}}$$

Where, Time is for the total hours of electrolysis during e-NRR, NH₃ yield is obtained from the

quantification of product after e-NRR

Therefore the TON and TOF for Ag₃PO₄ (2h) catalyst after 2 h of e-NRR is calculated as follows:

$$\text{TON} = \frac{0.02725}{0.02983} = 0.91$$

$$\text{TOF} = \frac{0.91}{2} = 0.46 \text{ h}^{-1}$$

Table S1a. Comparison of activity of recent reported catalysts towards e-NRR in different media					
Catalyst	Electrolyte	R_{NH3} (µg h^{-1} mg^{-1})	Pot. *vs.* RHE	F.E. (%)	Ref.
Ag nanosheets	0.1 M HCl	4.62×10^{-11} mol cm^{-2} s^{-1}	-0.6 V	4.8	6
Bi NPs	0.1 M Na₂SO₄	3.25 ± 0.08 µg cm^{-2} h^{-1} (-0.7 V)	-	12.11 ± 0.84% (-0.6 V)	7
B–Ag NSs	0.1 M HCl	26.48	-0.5 V	8.86	8
Fe doped-W₁₈O₄₉@CFP	0.25 M LiClO₄	24.7	-0.15 V	20.0 %	9
VN@NSC-900	0.1 M HCl	20.5	-0.3 V	8.6%	10
Pd-Ag-S PNSs	0.1 M Na₂SO₄	9.73	-0.2 V	18.41	11

Ce$_{1/3}$NbO$_3$	0.1 M Na$_2$SO$_4$	10.34 µg h^{-1} cm^{-2}	-0.8 V	6.87%	12
Ag NPs-rGO	0.1 M Na$_2$SO$_4$	18.86	-0.7 V	3.36	13
Ag NPs	0.1 M Na$_2$SO$_4$	9.23	-0.7 V	2.25	13
FL-VS$_2$	0.1 M HCl	34.62	-0.7 V	2.09% (-0.6 V)	14
BD/Ag-AF	0.1 M Na$_2$SO$_4$	2.07 × 10^{-11} mol cm^{-2} s^{-1}	-0.6 V	7.36	15
SnNb$_2$O$_6$ nanosheets	0.5 M LiClO$_4$	53.1	-0.3 V	17.6%	16
Ag-Au@ZIF	0.2 M LiCF3SO3	1.0 9 10-11 mol s^{-1} cm^{-2}	-2.5 V *vs.* Ag/AgCl	18 ± 4	17
Ag triangular nanoplates	0.5 M K2SO4	58.5 mg h^{-1} g^{-1}	-0.25 V	25	18
MnMoO$_4$ nanorods/rGO	LiClO$_4$	60.3	-0.3 V	14.7%	19
Single Ag	0.1 M HCl	270.9	-0.6 V	21.9	20
AgNDs	0.1 M Na$_2$SO$_4$ (pH=10.5)	600.4 ± 23.0	-0.25 V	10.1 ± 0.7%	21
Mo–Co/NC	0.1 M Na$_2$SO$_4$	89.8 µmol h^{-1} g$_{cat.}^{-1}$	-0.1 V	13.5%	22
Ag$_3$Cu BPNs	0.1 M Na$_2$SO$_4$	24.59	-0.5 V	13.28	23
Mo-MnO$_2$ NFs	0.1 M Na$_2$SO$_4$	36.6 (-0.5 V)	-	12.1% (-0.4 V)	24
Cu–TiO$_2$/CP	0.5 M LiClO$_4$	21.31	-0.55 V	21.99%	25
FeVO$_4$	0.5 M LiClO$_4$	52.8 (-0.4 V)	-	15.7% (-0.3 V)	26
La$_x$FeO$_{3-\delta}$	0.1 M Li$_2$SO$_4$	22.1 (-0.5 V)	-	25.6% (-0.3 V)	27
CoP$_3$/CC	0.1 M Na$_2$SO$_4$	3.61 × 10^{-11} mol s^{-1} cm^{-2}	-0.2 V	11.94%	28
Au(111)@Bi$_2$S$_3$	Na$_2$SO$_4$	45.57	-0.8 V	3.10%	29
SnS@C	0.1 M Na$_2$SO$_4$	24.33	-0.5 V	14.56%	30
Ag$_3$PO$_4$ (2 h)	**0.1 M KOH**	**456.75**	**0 V**	**26.66**	**This work**

Ag$_3$PO$_4$ (4 h)	0.1 M KOH	335.23	-0.1 V	19.57	This work
Ag$_3$PO$_4$ (6 h)	0.1 M KOH	527.99	0 V	20.87	This work

Table S1b. Comparison of activity of recent reported catalysts towards NRR in alkaline media					
Catalyst	Electrolyte	R_{NH3} (μg h^{-1} mg$_{cat.}^{-1}$)	Pot. *vs.* RHE	F.E. (%)	Ref.
MIL-100 (Al)/Cu	0.1 M KOH	10.6 μg h^{-1} cm^{-2} mg$_{cat.}^{-1}$	0 V	22.6	31
Ag$_2$Au$_1$	0.1 M KOH	21.7	-0.3 V	3.8	32
Co$_3$Fe–MOF	0.1 M KOH	8.79	-0.2 V	25.64	33
3D Rh particles	0.1 M KOH	35.58	−0.2 V	1.2 (0 V)	34
Fe–N/C–carbon nanotube (CNT)	0.1 M KOH	34.83	-0.2 V	9.28	35
Cu SAC	0.1 M KOH	53.3	-0.35 V	13.8	36
Cu/PI-300	0.1 M KOH	12.4 μg h^{-1} cm^{-2}	-0.3 V	6.56	37
FeSA-N-C	0.1 M KOH	7.48 μg h^{-1} cm^{-2}	0 V	56.55	38
C-ZIF-1100-1 h	0.1 M KOH	9.22 mmol g^{-1} h^{-1}	-0.3 V	10.2	39
SA-Mo/NPC	0.1 M KOH	34.0 g h^{-1} mg$_{cat}^{-1}$	-0.45 V	14.6	40
PdRu TPs	0.1 M KOH	37.23	-0.2 V	1.85	41
Pd$_3$Cu$_1$	0.1 M KOH	39.9	-0.25 V	0.58	42
Rh NNs	0.1 M KOH	23.9	-0.2 V	0.217	43
Pd$_{0.2}$Cu$_{0.8}$/rGO	0.1 M KOH	2.80	-0.2 V	-	44
Se-doped C	0.1 M KOH	1.14 μg h^{-1} cm^{-2}	-0.45V	3.92	45

|					
Te-doped C	0.1 M KOH	1.91 µg h^{-1} cm^{-2}	-0.5 V	4.6	45
FeWS$_x$@FeWO$_4$-2	1 M KOH	16.6	-0.45 V	6.01	46
Eex-COF/NC	0.1 M KOH	12.5	-0.2V	45.4	47
Ru@Ti3C2Tx	0.1 M KOH	2.3 µmol h^{-1} cm^{-2}	-0.4 V	13.13	48
Cu@Ti3C2Tx	0.1 M KOH	3.04 µmol h^{-1} cm^{-2}	-0.5 V	7.31	49
Au/CeOx-RGO	0.1 M KOH	8.31	-0.2 V	10.1	50
CuAg@Ti3C2 Tx	0.1 M KOH	4.12 µmol cm^{-2} h^{-1}	-0.5 V	9.77	51
Tetrahexahedral Au nanorods	0.1 M KOH	6.042	-0.2 V	3.88	52
CoP hollow nanocage	1 M KOH	10.78	-0.4 V	7.36	53
Fe3Mo3C	1 M KOH	13.1 µg cm^{-2} h^{-1}	-0.5 V	0.26	2
FL-Sb nanosheets	0.1 M KOH	133.1	0.05 V	11.6	54
2D Layered W2N3	0.1 M KOH	11.66	-0.2 V	11.67	55
CoPi/NPCS	0.1 M KOH	20.5	-0.2 V	7.07	56
K2Ti4O9 nanobelt	0.1 M KOH	22.8	-0.5 V	5.9	57
Zr-doped TiO2	0.1 M KOH	8.9 µg h^{-1} cm^{-2}	-0.45 V	17.3	58
CoPi/HSNPC	0.1M KOH	16.48	-0.2 V	4.46	59
Cu$_{1.81}$S	0.1 M KOH	2.19 µmol h^{-1} cm^{-2}	-0.1 V	14.1	60
Co/C-900	0.1 M KOH	4.66 µmol h^{-1} cm^{-2}	-0.3 V	11.53	61
Ag$_3$PO$_4$ (2 h)	**0.1 M KOH**	**456.75**	**0 V**	**26.66**	**This work**
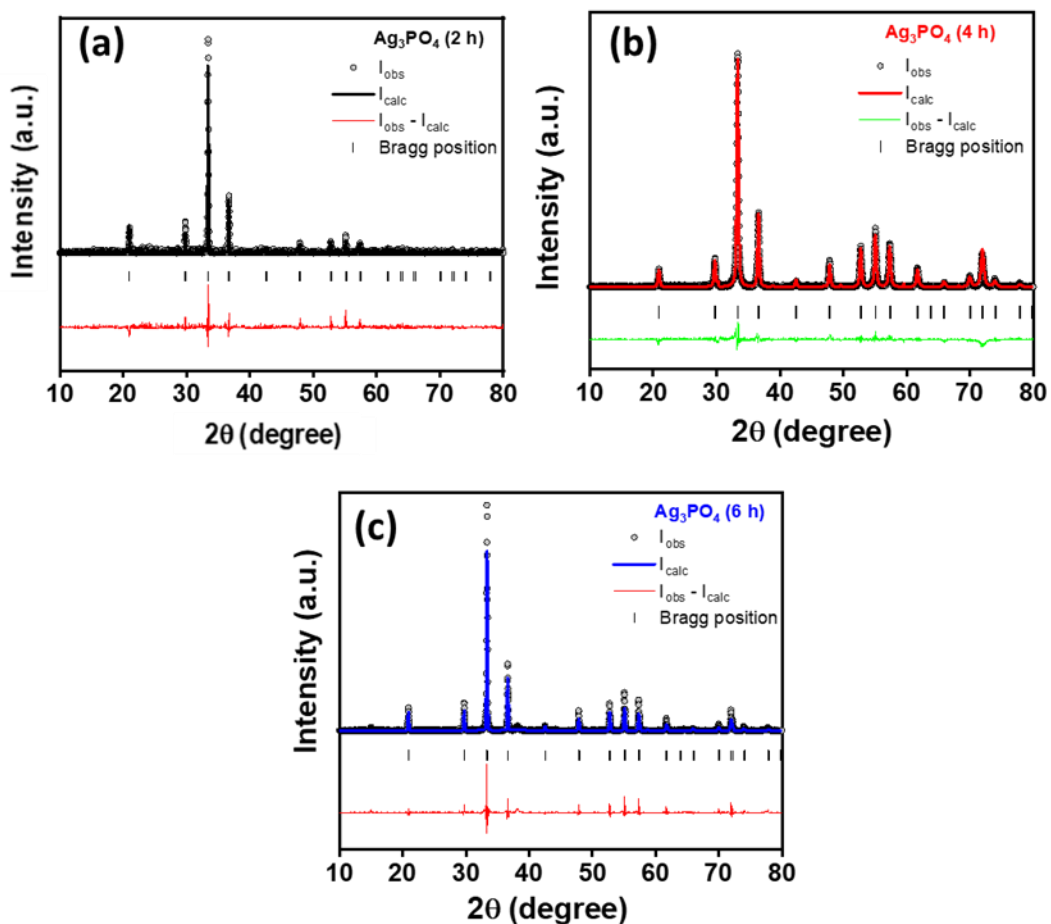
Fig. S6 Powder-XRD patterns for (a) Ag₃PO₄ (2 h); Goodness of fit: 4.986, (c) Ag₃PO₄ (4 h); Goodness of fit: 3.2 and (d) Ag₃PO₄ (6 h) electrocatalysts Goodness of fit: 8.929.

Table S2. EDS composition analysis						
Ag₃PO₄ (2 h)			Ag₃PO₄ (4 h)		Ag₃PO₄ (6 h)	
Element	Weight%	Atomic%	Weight%	Atomic%	Weight%	Atomic%
O K	23.31	62.14	26.55	66.08	28.47	70.83
P K	7.69	10.58	7.43	9.55	3.03	3.90
Ag L	69.00	27.28	66.01	24.37	68.50	25.27
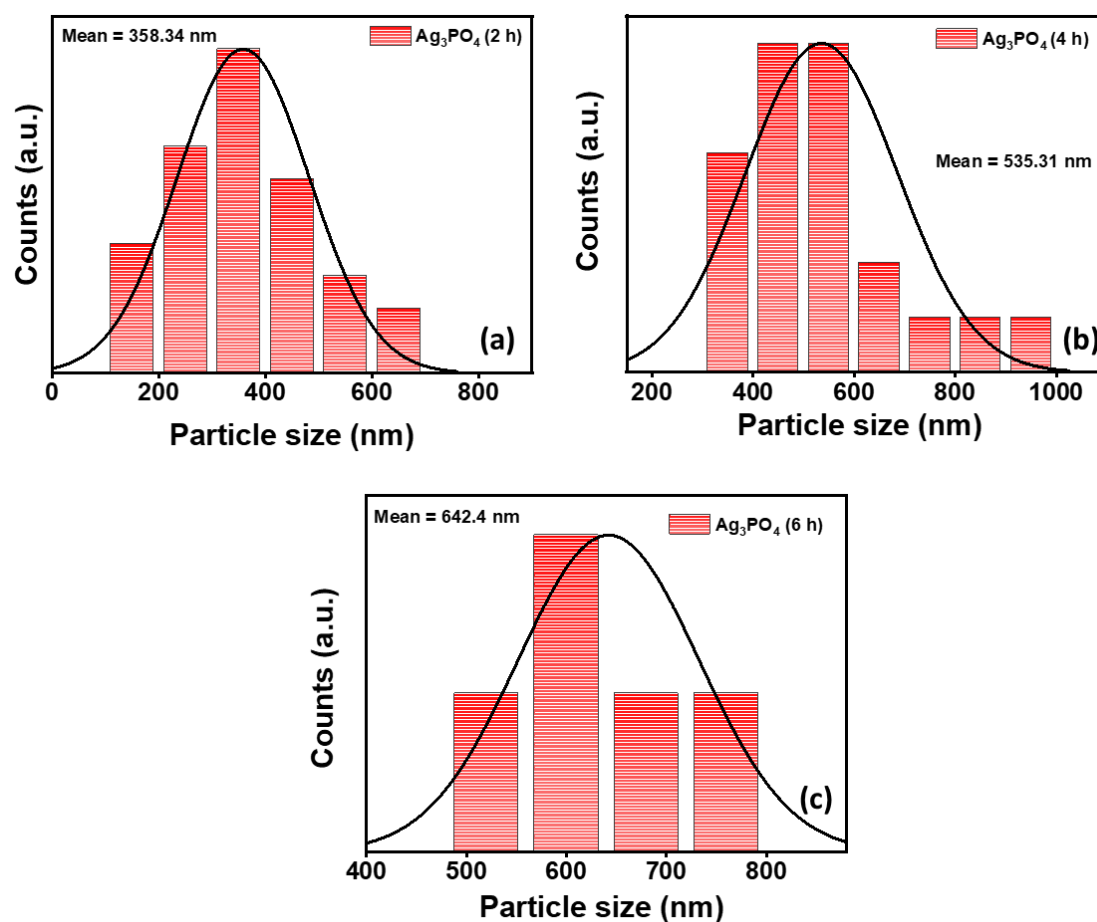
Fig. S7A Particle size distribution histogram of (a) Ag_3PO_4 (2 h), (b) Ag_3PO_4 (4 h) and (c) Ag_3PO_4 (6 h) catalyst from corresponding FE-SEM images.
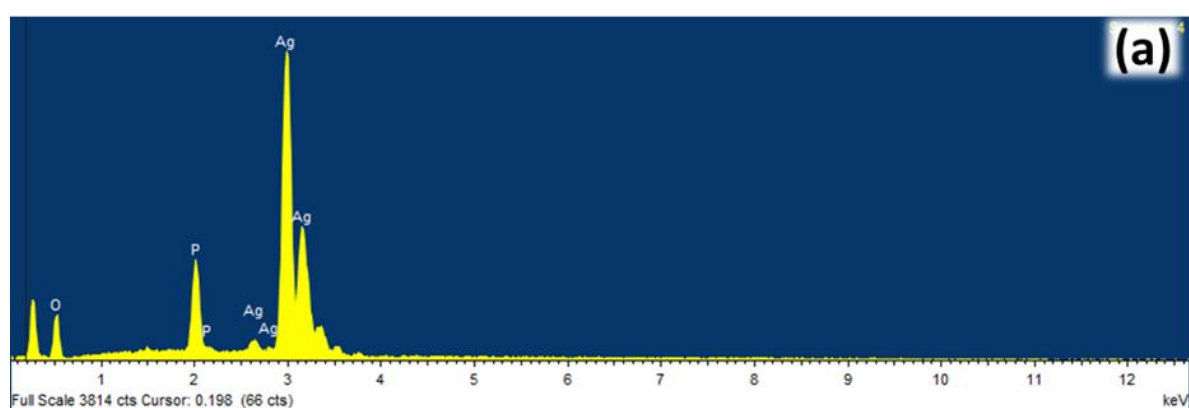
Fig. S7B EDS spectrum of (a) Ag_3PO_4 (2 h) catalyst.

S. No.	Electrocatalyst	R_s (Ω)	R_p (Ω)	R_{ct} (Ω)
	Table S3. Electrochemical Impedance analysis extracted from Fig. 3a.			
1	Ag_3PO_4 (2 h)	0.95	70.98	70.03
2	Ag_3PO_4 (4 h)	0.12	108.64	108.52
3	Ag_3PO_4 (6 h)	0.12	80.11	79.99

Electrochemical impedance measurements

The electrochemical impedance behavior was studied for the composites in N_2-saturated 0.1M KOH electrolyte by applying 0.880 V *vs.* Ag/AgCl of DC potential over an AC perturbation of 10 mV with logarithmic frequency step over a single sine wave for the various frequency ranging from 20 Hz to 600 kHz in the logarithmic steps. The solution resistance (R_s) was obtained from the point of intersection of the semicircle at the high frequency real axis whereas the polarization resistance (R_p) at the low frequency near the electrode-electrolyte interface. The charge transfer resistance (R_{ct}) was calculated by subtracting the R_s from R_p.
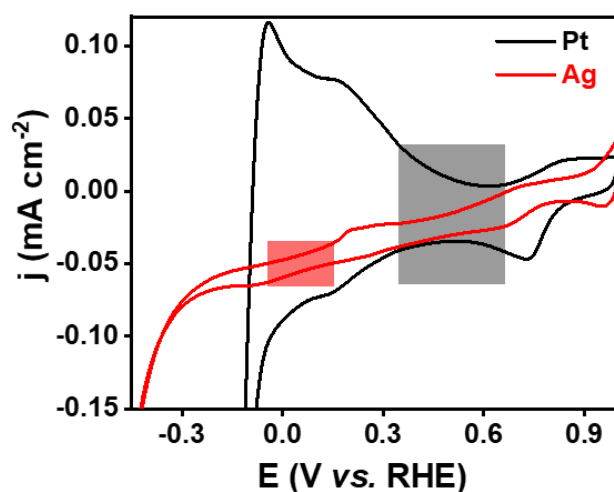
Fig. S8 Cyclic voltammograms for Pt and Ag separately for non-faradaic region determination.

Double-layer pseudo-capacitance (C_{dl}):

To determine the double-layer pseudo-capacitance (C_{dl}) of the composites, the cyclic voltammetry was performed in the non-faradic potential region 0.88 V and 0.98 V *vs.* RHE with different scan rate (10 to 320 mV s^{-1}). The double layer pseudo capacitance was obtained as the slope of the graph of both anodic and cathodic averaged out current density versus the scan rate.
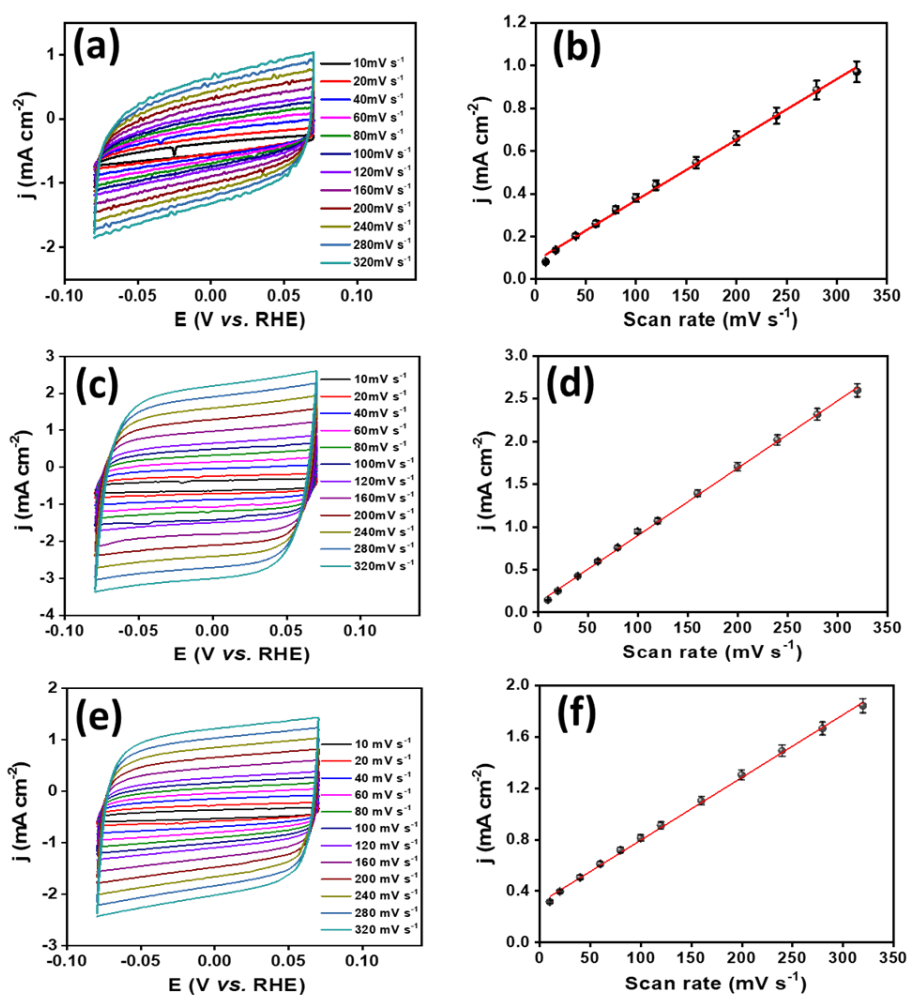

Fig. S9. Cyclic voltammogram **(a)** Ag$_3$PO$_4$ (2 h), **(b)** Ag$_3$PO$_4$ (4 h), **(c)** Ag$_3$PO$_4$ (6 h) in non-faradic potential region (H$_{UPD}$ region for Ag determined from Fig. S8) at various scan rates where **(d)**, **(e)** & **(f)** are corresponding average current density versus scan rate plot for ECSA determination in 0.1 M KOH. CE: Pt wire; RE: Hg/HgO/1 M NaOH.

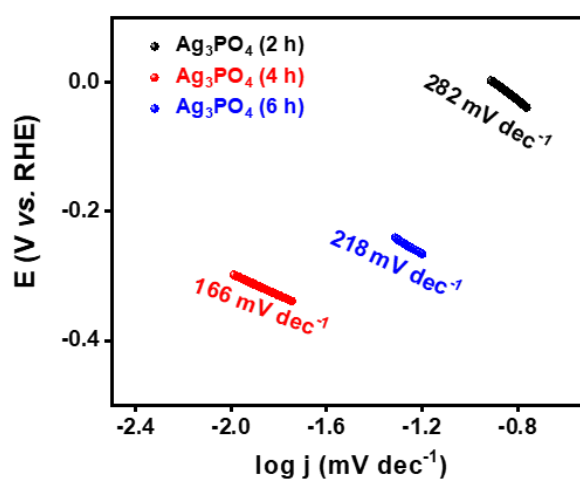| Table S4. Electrochemical surface area (ECSA) determination from Fig. S9.			
S.No.	Electrocatalyst	C_{dl}* (mF)	ECSA (cm^2)
1	Ag$_3$PO$_4$ (2 h)	2.83 at 0 V *vs.* RHE	70.75
2	Ag$_3$PO$_4$ (4 h)	7.88 at 0 V *vs.* RHE	197
3	Ag$_3$PO$_4$ (6 h)	4.87 at 0 V *vs.* RHE	121.75

Fig. S10 Tafel plots for Ag$_3$PO$_4$ catalysts under Ar-saturated electrolyte environment for HER.

Table S5. Tafel slope values extracted from LSV of catalysts			
S.No.	Electrocatalyst	Tafel slope (mV dec^{-1}) for HER	Tafel slope (mV dec^{-1}) for e-NRR
1	Ag$_3$PO$_4$ (2 h)	282	229
2	Ag$_3$PO$_4$ (4 h)	166	394
3	Ag$_3$PO$_4$ (6 h)	218	297
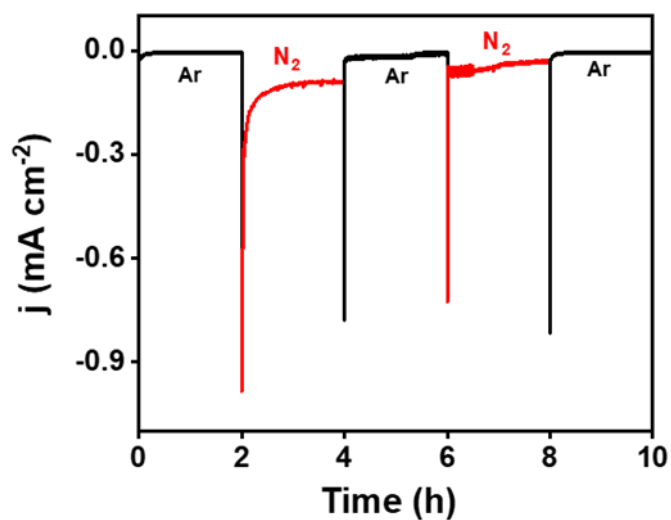
Fig. S11 Chronoamperometry measurements in Ar and N_2 saturated 0.1 M KOH.
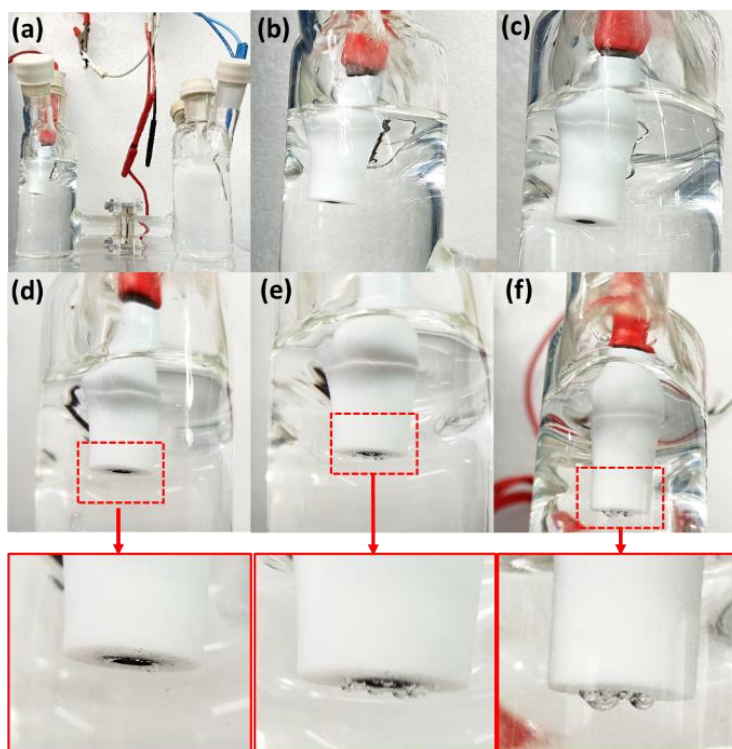

Fig. S12 (a) Photographs of Ag_3PO_4 (2 h) captured during GC analysis for HER quantification at different potentials (b) 0 V, (c) -0.1 V, (d) -0.2 V, (e) -0.3 V, (f) -0.4 V respectively.

Determination of HER productions:

Evolution of H_2 during NRR at applied potentials were detected quantitatively by means of a gas chromatograph (GC, SHIMADZU, GC-2030) During NRR, high purity N_2 (99.999%) was continuously purged in the cathodic chamber of H-cell. A SHIMADZU Rt-Q-BOND column was installed in GC having two detectors, namely, a thermal conductivity detector (TCD) and a flame ionization detector (FID) to measure H_2. The carrier gas used was N_2. Below mentioned are the formulas used for quantification of produced hydrogen.

$$\text{Yield rate (mmol mg}^{-1}\text{ h}^{-1}) = \frac{\text{yield (mmol)}}{\text{t (h)} \times \text{m}_{cat.}\text{(mg)}}$$

$$\text{Selectivity (\%)} = \frac{\text{Experimental}_{H2} \times 100}{\text{Theoretical}_{H2}}$$
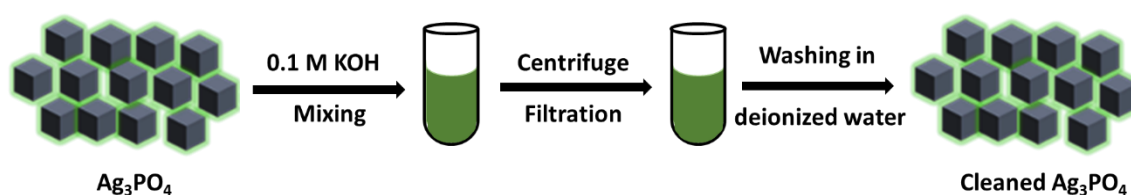
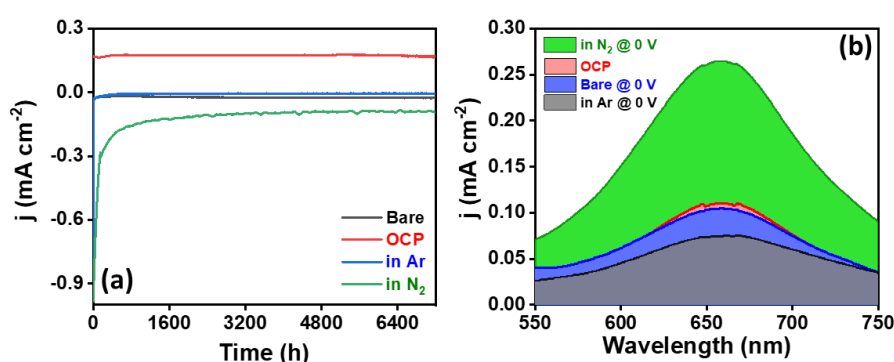**Scheme S1.** Schematic representation of catalyst treatment for NO_3^- removal.

Fig. S13 (a) Chronoamperometric curves and (b) UV-vis spectrum of Ag_3PO_4 (2 h) at OCP in N_2 saturated 0.1 M KOH, at 0.0 V *vs.* RHE in N_2/Ar saturated electrolyte, and that of bare GC at 0.0 V *vs.* RHE in N_2 saturated 0.1 M KOH respectively.

Nitrate (NO$_3^-$) and nitrite (NO$_2^-$) determination[62]:

For determination of any trace amount of NO$_3^-$ present in the electrolyte (i.e. 0.1 M KOH), UV-Vis. spectrophotometry was utilised wherein the peak at wavelength of 220 nm correspond to absorption of nitrates. Furthermore, the nitrate amount was quantified with respect to measured absorbance value. Standard solutions were prepared using NaNO$_3$ stock solution with varying concentrations i.e. 0.2 ppm to 5 ppm. Subsequently, 5 mL of standard along with sample solution were taken in glass vial to which 0.1 mL of 1 M HCl was added later on with recurrent shaking. The solution kept undisturbed for 5 min. and UV-vis. measurement was performed in the range of 200-300 nm from which the calibration curve was acquired. Additionally, quantification of nitrites can be performed via diazotization reaction by using sulphanilamide under acidic environment followed by coupling with N-(1-Napthyl) ethylenediamine dihydrocholoride which result into formation of pink colored azo dyes with corresponding peak at 540 nm respectively. Initially, standard solutions were prepared using NaNO$_2$ stock solution with different concentrations i.e. 2 to 60 µg L^{-1}. Afterwards, two reagents were prepared separately; 0.5 g of sulphanilamide in 50 mL of 2 M HCl i.e. **A** and 20 mg of N-(1-Napthyl) ethylenediamine dihydrocholoride in 20 mL of deionized H$_2$O i.e. **B**. Briefly, 5 mL of standard or sample solution were taken in glass vials followed by addition of 0.1 mL of A which was then allowed to stand for 10 min. Afterwards, 0.1 mL of B was added to above solution respectively. The solution mixture was kept undisturbed for 30 min and

amount of NO_2^- was estimated under wavelength range of 440-600 nm, from which calibration curves were extracted.
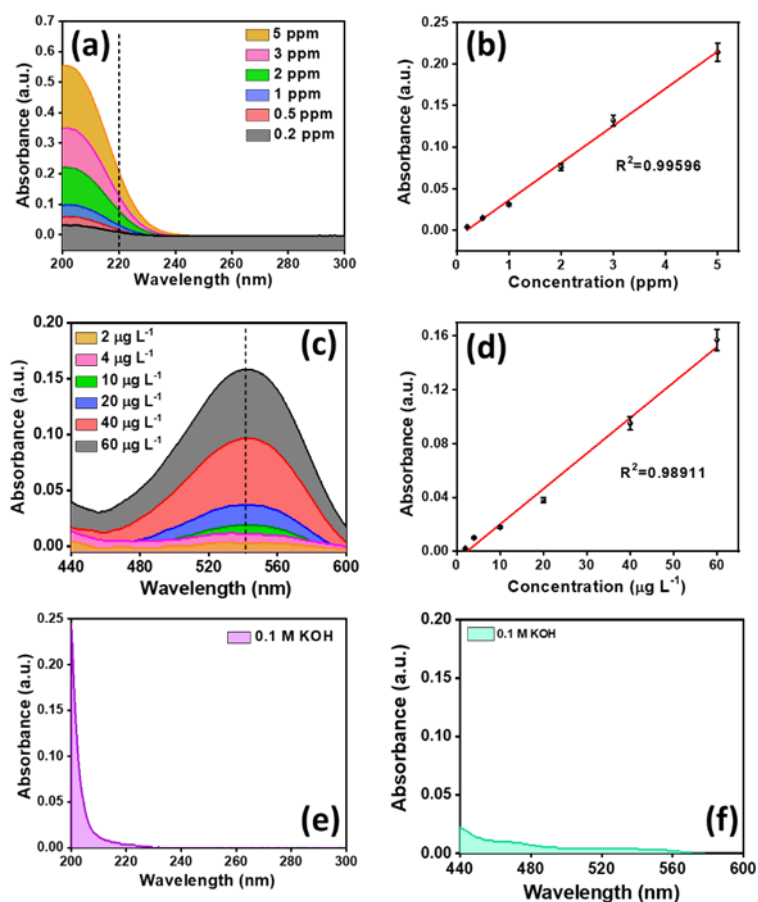

Fig. S14 UV-vis spectrum and corresponding calibration curve for **(a-b)** nitrate and **(c-d)** nitrite detection. Detection of amount of **(e)** NO_3^- and **(f)** NO_2^- in electrolyte solution.
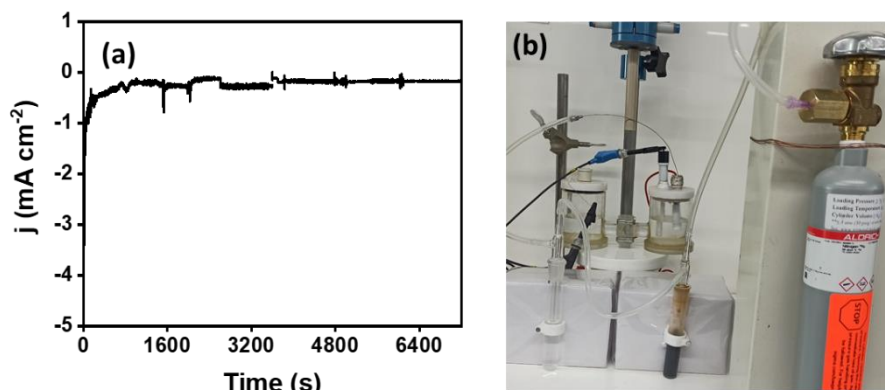
Fig. S15 (a) Chronoamperometry measurements at 0 V (*vs.* RHE) by Ag₃PO₄ (2 h) in $^{15}N_2$ saturated electrolyte solution and (b) photographic representation of cell setup acquired during isotope labelling measurements.

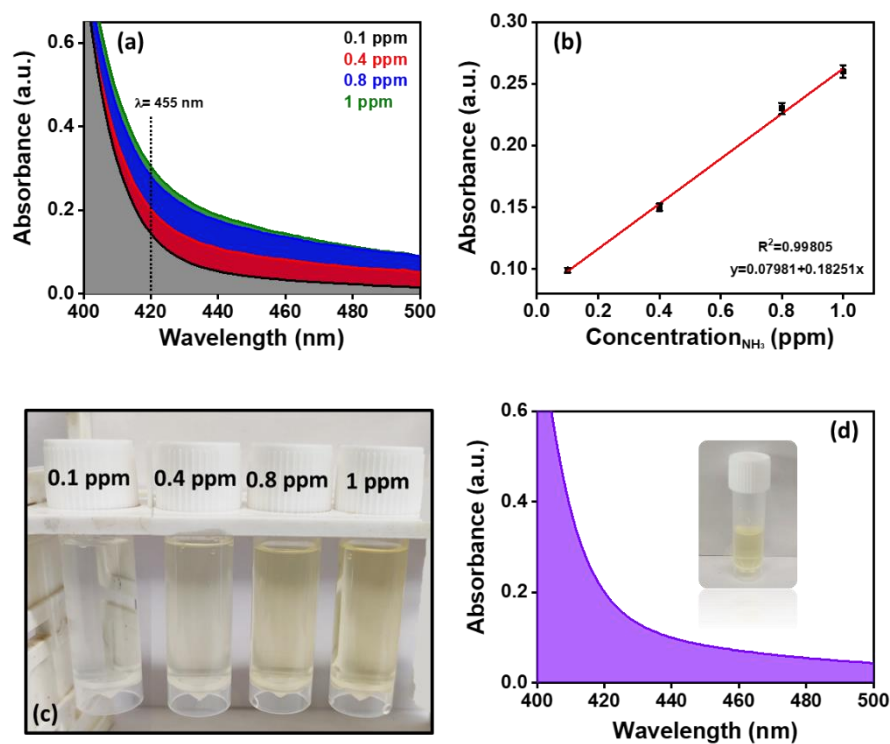**Fig. S16** (a) UV-Vis. curves acquired for standard NH_4^+ solutions after Nessler's reagent test and (b) corresponding calibration curve for quantification of NH_3 in samples. (c) Images showing color development of standard NH_4^+ solutions after Nessler's test. (d) UV-Vis. curve for electrolyte sample solution collected after 2 h of NRR by Ag₃PO₄ (2 h) in N_2-saturated 0.1 M KOH.
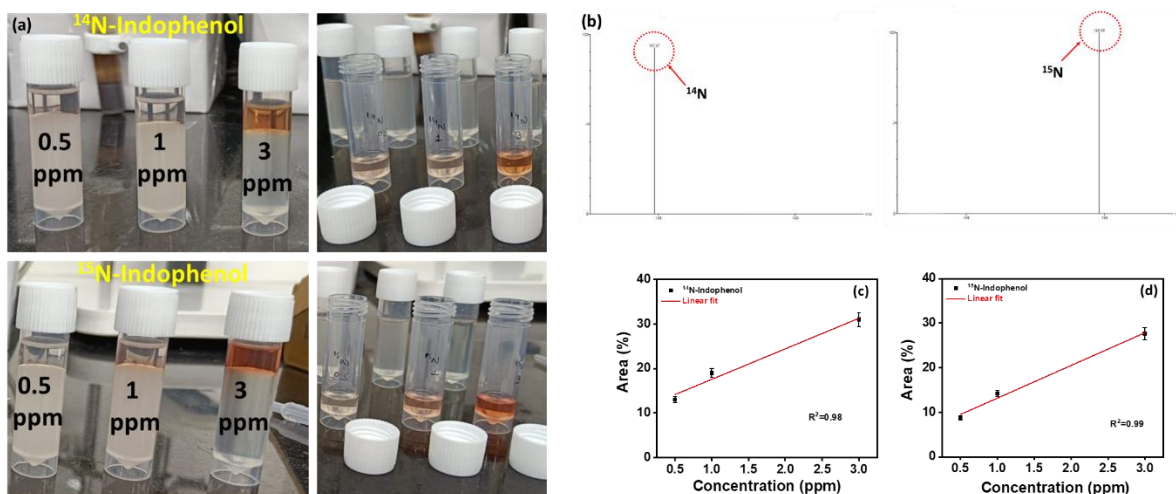
Fig. S17 (a) Photographs showing the extraction of Indophenol red from organic layer before LC-MS quantification for standard samples, abundance of (b) ^{14}N Indophenol and ^{15}N Indophenol for the electrolyte samples obtained after NRR. (c-d) Calibration curves extracted from LC-MS of standard samples after Berthelot reaction.

Table S6A. Comparison of NH$_3$ yield rates obtained after 2 h of e-NRR by Ag$_3$PO$_4$ (2 h) at 0 V (*vs.* RHE).

S.No.	NH$_3$ detection method	NH$_3$ yield rate (μg h^{-1} mg$_{cat.}^{-1}$)
1.	Indophenol Blue	456.75
2.	Nessler's reagent	435.80

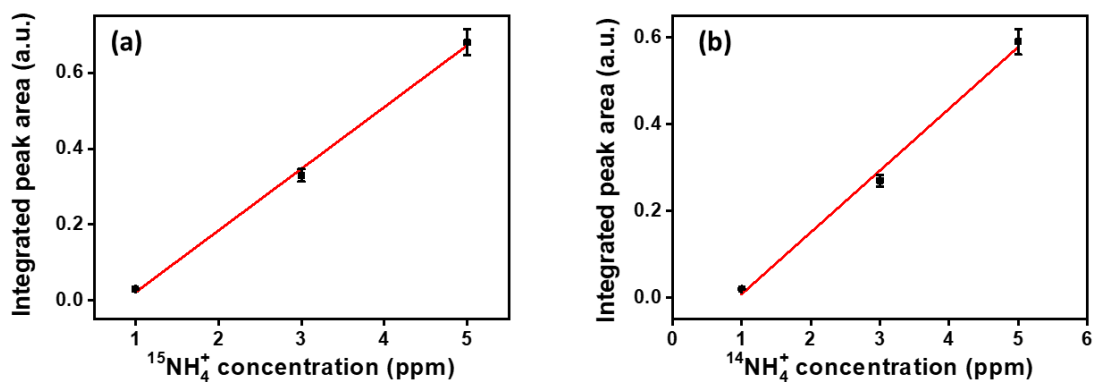| Table S6B. Comparison of NH$_3$ yield rates obtained after 2 h of e-NRR by Ag$_3$PO$_4$ (2 h) at 0 V (*vs.* RHE) by LC-MS (isotope labelling experiment)		
S.No.	Electrolyte sample	NH$_3$ yield rate (μg h^{-1} mg$_{cat.}^{-1}$)
1.	^{14}N-Indophenol	479.38
2.	^{15}N-Indophenol	455.08

Fig. S18 (a) Calibration curves for different NH_4^+ concentration extracted from ^1H NMR spectra

in Fig. 6d for (a) $^{15}NH_4^+$ and (b) $^{14}NH_4^+$ respectively.

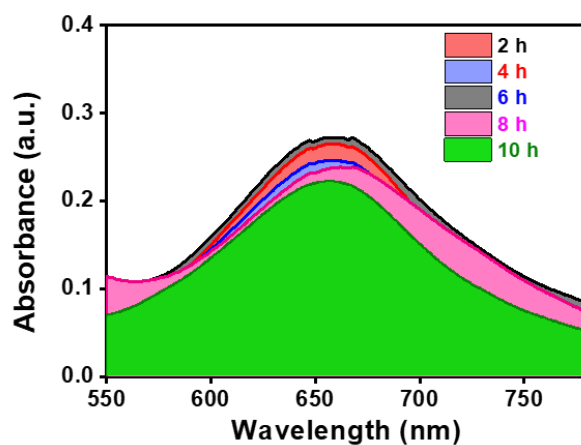| Table S6C. Comparison of NH_3 yield rates obtained after 2 h of e-NRR by Ag_3PO_4 (2 h) at 0 V (*vs.* RHE) by ^1H-NMR (isotope labelling experiment)		
S.No.	**Electrolyte sample**	**NH_3 yield rate ($\mu g\ h^{-1}\ mg_{cat.}^{-1}$)**
1.	$^{14}NH_4^+$	460
2.	$^{15}NH_4^+$	410

Fig. S19 UV-vis spectrum for electrolyte sample collected after chronoamperometry for

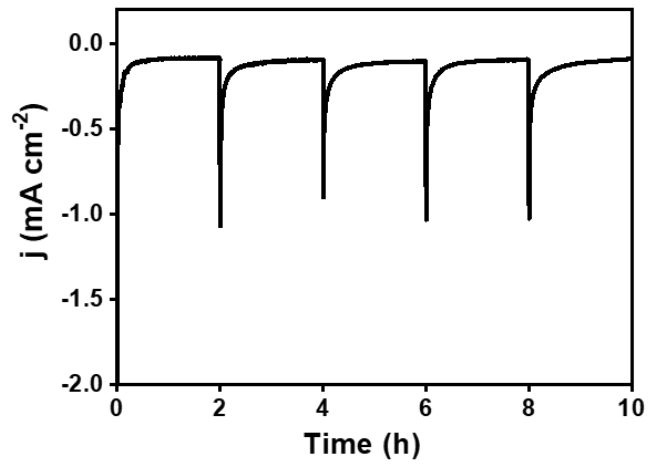different cycles of 2 hrs by Ag_3PO_4 (2 h).

Fig. S20A Stability test of Ag$_3$PO$_4$ (2 h) at 0.0 V *vs.* RHE for 10 h in N$_2$ saturated 0.1 M KOH.
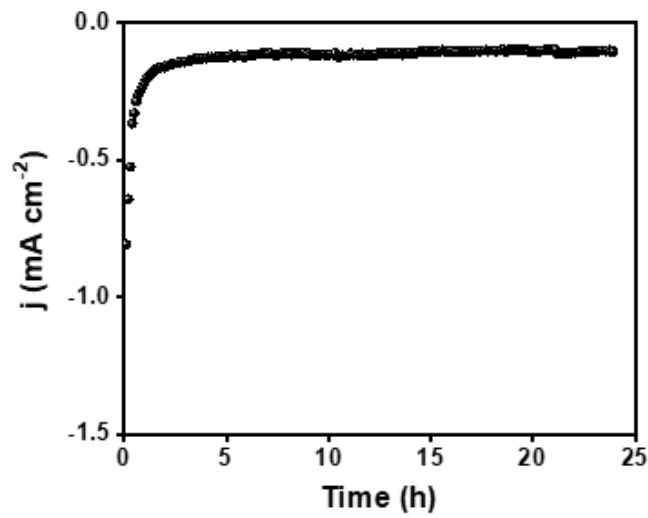

Fig. S20B Chronoamperometry curve acquired after 24 h continuous NRR in N$_2$-saturated 0.1
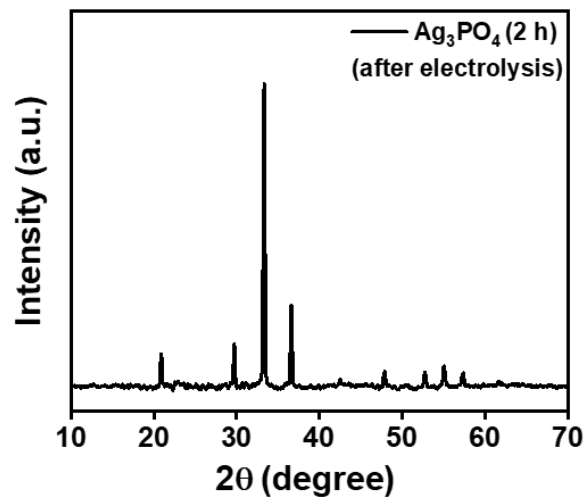
M KOH.

Fig. S21 Post-stability X-ray diffraction pattern for Ag$_3$PO$_4$ (2 h) after 10 h electrolysis in 0.1 M

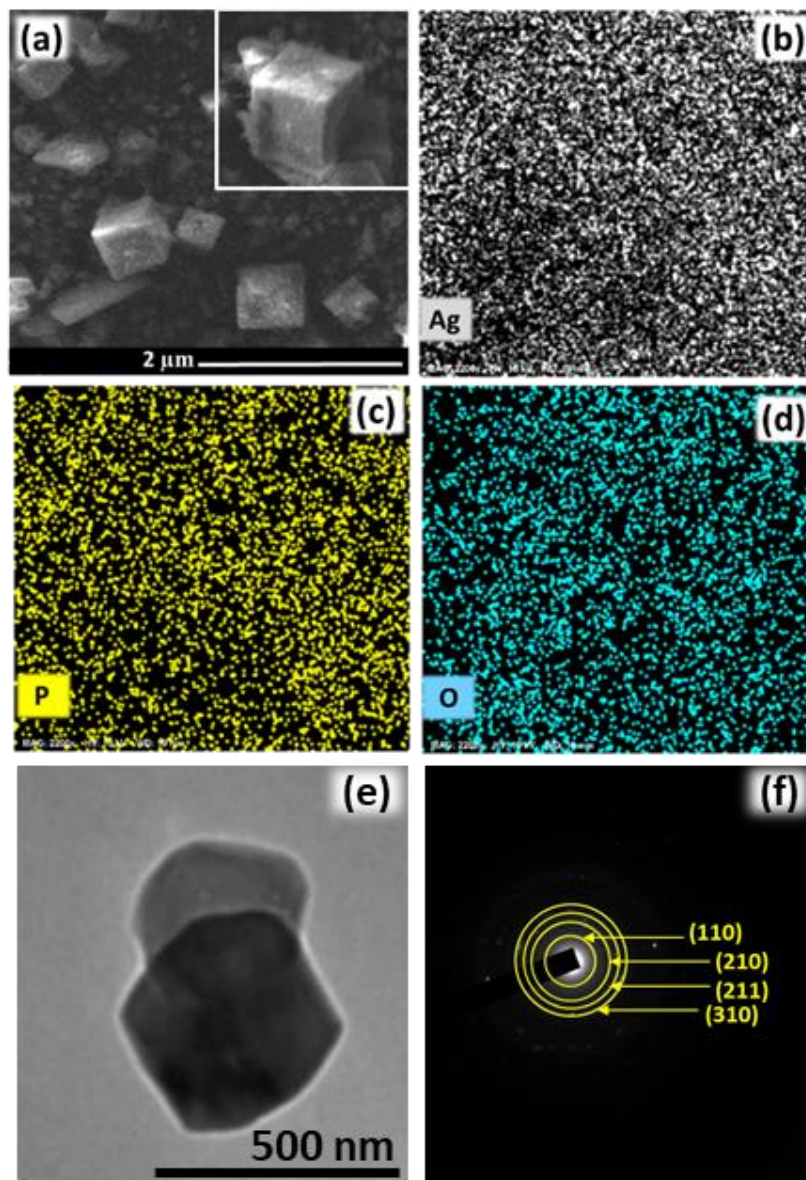KOH electrolyte.

Fig. S22 (a) SEM image and (b-d) EDX dot mapping for all respective elements in Ag_3PO_4 (2 h) post-stability measurements. (e) TEM image of Ag_3PO_4 (2 h) catalyst and (f) corresponding SAED pattern after NRR stability tests.
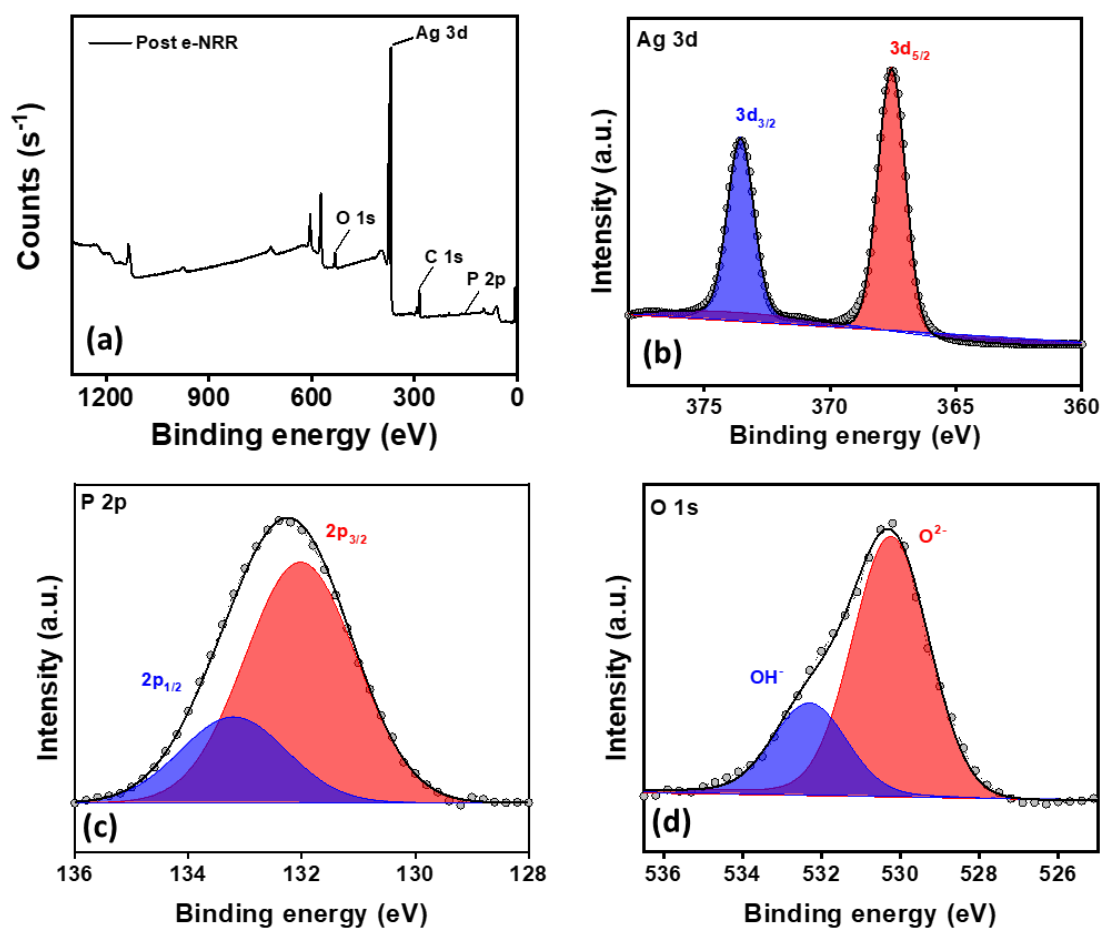
Fig. S23 Post e-NRR stability (a) survey spectrum and XP deconvoluted (a) Ag 3d, (b) P 2p and

(c) O 1s spectra of Ag$_3$PO$_4$ (2 h).

Table S7: Post EDS composition analysis of Ag$_3$PO$_4$ (2 h)				
Before			**After**	
Element	**Weight%**	**Atomic%**	**Weight%**	**Atomic%**
O K	23.31	62.14	25.18	64.47
P K	7.69	10.58	7.54	9.98
Ag L	69.00	27.28	67.28	25.55

References

1. Y. Zhao, R. Shi, X. Bian, C. Zhou, Y. Zhao, S. Zhang, F. Wu, G. I. Waterhouse, L. Z. Wu and C. H. Tung, *Adv. Sci.*, 2019, **6**, 1802109.

2. H. Cheng, P. Cui, F. Wang, L. X. Ding and H. Wang, *Angew. Chem.*, 2019, **131**, 15687-15693.

3. C. Tang and S.-Z. Qiao, *Joule*, 2019, **3**, 1573-1575.

4. S. Z. Andersen, V. Čolić, S. Yang, J. A. Schwalbe, A. C. Nielander, J. M. McEnaney, K. Enemark Rasmussen, J. G. Baker, A. R. Singh and B. A. Rohr, *Nature*, 2019, **570**, 504-508.

5. S. E. Saji, H. Lu, Z. Lu, A. Carroll and Z. Yin, *Small Methods*, 2021, **5**, 2000694.

6. H. Huang, L. Xia, X. Shi, A. M. Asiri and X. Sun, *Chem. Commun.*, 2018, **54**, 11427-11430.

7. D. Yao, C. Tang, L. Li, B. Xia, A. Vasileff, H. Jin, Y. Zhang and S. Z. Qiao, *Adv. Energy Mater.*, 2020, **10**, 2001289.

8. Y. Li, H. Yu, Z. Wang, S. Liu, Y. Xu, X. Li, L. Wang and H. Wang, *Chem. Commun.*, 2019, **55**, 14745-14748.

9. Y. Tong, H. Guo, D. Liu, X. Yan, P. Su, J. Liang, S. Zhou, J. Liu, G. Q. Lu and S. X. Dou, *Angew. Chem. Int. Ed.*, 2020, **59**, 7356-7361.

10. X.-W. Lv, Y. Liu, Y.-S. Wang, X.-L. Liu and Z.-Y. Yuan, *Appl. Catal. B Environ.*, 2021, **280**, 119434.

11. H. Wang, S. Liu, H. Zhang, S. Yin, Y. Xu, X. Li, Z. Wang and L. Wang, *Nanoscale*, 2020.

12. Hu, Y. Sun, S. Guo, J. Sun, Y. Fu, S. Chen, S. Zhang and J. Zhu, *Appl. Catal. B Environ.*, 2021, **280**, 119419.

13. N. Khaliq, M. A. Rasheed, G. Cha, M. Khan, S. Karim, P. Schmuki and G. Ali, *Sens. Actuators B Chem.*, 2020, **302**, 127200.

14. L. Zhao, R. Zhao, Y. Zhou, X. Wang, X. Chi, Y. Xiong, C. Li, Y. Zhao, H. Wang and Z. Yang, *J. Mater. Chem. A*, 2021, **9**, 24985-24992.

15. L. Ji, X. Shi, A. M. Asiri, B. Zheng and X. Sun, *Inorg. Chem.*, 2018, **57**, 14692-14697.

16. X. Li, Y. Tian, X. Wang, Y. Guo and K. Chu, *Sustain. Energy Fuels*, 2021, **5**, 4277-4283.

17. H. K. Lee, C. S. L. Koh, Y. H. Lee, C. Liu, I. Y. Phang, X. Han, C.-K. Tsung and X. Y. Ling, *Sci. Adv.*, 2018, **4**, eaar3208.

18. W.-Y. Gao, Y.-C. Hao, X. Su, L.-W. Chen, T.-A. Bu, N. Zhang, Z.-L. Yu, Z. Zhu and A.-X. Yin, *Chem. Commun.*, 2019, **55**, 10705-10708.

19. Y. Liu, Y. Luo, Q. Li, J. Wang and K. Chu, *Chem. Commun.*, 2020, **56**, 10227-10230.

20. Y. Chen, R. Guo, X. Peng, X. Wang, X. Liu, J. Ren, J. He, L. Zhuo, J. Sun and Y. Liu, *ACS Nano*, 2020.

21. W. Li, K. Li, Y. Ye, S. Zhang, Y. Liu, G. Wang, C. Liang, H. Zhang and H. Zhao, *Commun. Chem.*, 2021, **4**, 1-11.

22. L. Ma, Z. Bi, Y. Xue, W. Zhang, Q. Huang, L. Zhang and Y. Huang, *J. Mater. Chem. A*, 2020, **8**, 5812-5842.

23. H. Yu, Z. Wang, D. Yang, X. Qian, Y. Xu, X. Li, H. Wang and L. Wang, *J. Mater. Chem. A*, 2019, **7**, 12526-12531.

24. K. Chu, Y.-p. Liu, Y.-b. Li, Y.-l. Guo, Y. Tian and H. Zhang, *Appl. Catal. B Environ.*, 2020, **264**, 118525.

25. T. Wu, H. Zhao, X. Zhu, Z. Xing, Q. Liu, T. Liu, S. Gao, S. Lu, G. Chen and A. M. Asiri, *Adv. Mater.*, 2020, **32**, 2000299.

26. P. Shen, Y. Liu, Q. Li and K. Chu, *Chem. Commun.*, 2020, **56**, 10505-10508.

27. K. Chu, F. Liu, J. Zhu, H. Fu, H. Zhu, Y. Zhu, Y. Zhang, F. Lai and T. Liu, *Adv. Energy Mater.*, 2021, **11**, 2003799.

28. J. Gao, X. Lv, F. Wang, Y. Luo, S. Lu, G. Chen, S. Gao, B. Zhong, X. Guo and X. Sun, *J. Mater. Chem. A*, 2020, **8**, 17956-17959.

29. L. Zhao, J. Zhou, L. Zhang, X. Sun, X. Sun, T. Yan, X. Ren and Q. Wei, *ACS Appl. Mater. Interfaces*, 2020, **12**, 55838-55843.

30. W. Yu, F. Shu, Y. Huang, F. Yang, Q. Meng, Z. Zou, J. Wang, Z. Zeng, G. Zou and S. Deng, *J. Mater. Chem. A*, 2020, **8**, 20677-20686.

31. Y. Fu, K. Li, M. Batmunkh, H. Yu, S. Donne, B. Jia and T. Ma, *ACS Appl. Mater. Interfaces*, 2020, **12**, 44830-44839.

32. Q. Zhang, Y. Shen, Y. Hou, L. Yang, B. Chen, Z. Lei and W. Zhang, *Electrochim. Acta*, 2019, **321**, 134691.

33. W. Li, W. Fang, C. Wu, K. N. Dinh, H. Ren, L. Zhao, C. Liu and Q. Yan, *J. Mater. Chem. A*, 2020, **8**, 3658-3666.

34. T. Chen, S. Liu, H. Ying, Z. Li and J. Hao, *Chem. Asian J.*, 2020, **15**, 1081-1087.

35. Y. Wang, X. Cui, J. Zhao, G. Jia, L. Gu, Q. Zhang, L. Meng, Z. Shi, L. Zheng and C. Wang, *ACS Catal.*, 2018, **9**, 336-344.

36. W. Zang, T. Yang, H. Zou, S. Xi, H. Zhang, X. Liu, Z. Kou, Y. Du, Y. P. Feng and L. Shen, *ACS Catal.*, 2019, **9**, 10166-10173.

37. Y.-X. Lin, S.-N. Zhang, Z.-H. Xue, J.-J. Zhang, H. Su, T.-J. Zhao, G.-Y. Zhai, X.-H. Li, M. Antonietti and J.-S. Chen, *Nat. Commun.*, 2019, **10**, 1-7.

38. M. Wang, S. Liu, T. Qian, J. Liu, J. Zhou, H. Ji, J. Xiong, J. Zhong and C. Yan, *Nat. Commun.*, 2019, **10**, 341.

39. S. Mukherjee, D. A. Cullen, S. Karakalos, K. Liu, H. Zhang, S. Zhao, H. Xu, K. L. More, G. Wang and G. Wu, *Nano Energy*, 2018, **48**, 217-226.

40. L. Han, X. Liu, J. Chen, R. Lin, H. Liu, F. Lü, S. Bak, Z. Liang, S. Zhao and E. Stavitski, *Angew. Chem.*, 2019, **131**, 2343-2347.

41. H. Wang, Y. Li, C. Li, K. Deng, Z. Wang, Y. Xu, X. Li, H. Xue and L. Wang, *J. Mater. Chem. A*, 2019, **7**, 801-805.

42. F. Pang, Z. Wang, K. Zhang, J. He, W. Zhang, C. Guo and Y. Ding, *Nano Energy*, 2019, **58**, 834-841.

43. J. Zhang, X. Li, Y. Liu, Z. Zeng, X. Cheng, Y. Wang, W. Tu and M. Pan, *Nanoscale*, 2018, **10**, 11997-12002.

44. M. M. Shi, D. Bao, S. J. Li, B. R. Wulan, J. M. Yan and Q. Jiang, *Adv. Energy Mater.*, 2018, **8**, 1800124.

45. Y. Yang, L. Zhang, Z. Hu, Y. Zheng, C. Tang, P. Chen, R. Wang, K. Qiu, J. Mao and T. Ling, *Angew. Chem. Int. Ed.*, 2020, **59**, 4525-4531.

46. Y. Zhao, F. Li, W. Li, Y. Li, C. Liu, Z. Zhao, Y. Shan, Y. Ji and L. Sun, *Angew. Chem. Int. Ed.*, 2021, **60**, 20331-20341.

47. S. Liu, M. Wang, T. Qian, H. Ji, J. Liu and C. Yan, *Nat. Commun.*, 2019, **10**, 1-9.

48. Z. Xu, Y. Ying, G. Zhang, K. Li, Y. Liu, N. Fu, X. Guo, F. Yu and H. Huang, *J. Mater. Chem. A*, 2020, **8**, 26130-26138.

49. A. Liu, X. Liang, Q. Yang, X. Ren, M. Gao, Y. Yang and T. Ma, *ChemPlusChem*, 2021, **86**, 166-170.

50. Q. Zhang, C. Zhang, J. Liang, P. Yin and Y. Tian, *ACS Sustain. Chem. Eng.*, 2017, **5**, 3808-3818.

51. A. Liu, Q. Yang, X. Ren, M. Gao, Y. Yang, L. Gao, Y. Li, Y. Zhao, X. Liang and T. Ma, *Sustain. Energy*

Fuels, 2020, **4**, 5061-5071.

52. D. Bao, Q. Zhang, F. L. Meng, H. X. Zhong, M. M. Shi, Y. Zhang, J. M. Yan, Q. Jiang and X. B. Zhang, *Adv. Mater.*, 2017, **29**, 1604799.

53. W. Guo, Z. Liang, J. Zhao, B. Zhu, K. Cai, R. Zou and Q. Xu, *Small Methods*, 2018, **2**, 1800204.

54. M. Bat-Erdene, G. Xu, M. Batmunkh, A. S. Bati, J. J. White, M. J. Nine, D. Losic, Y. Chen, Y. Wang and T. Ma, *J. Mater. Chem. A*, 2020, **8**, 4735-4739.

55. H. Jin, L. Li, X. Liu, C. Tang, W. Xu, S. Chen, L. Song, Y. Zheng and S. Z. Qiao, *Adv. Mater.*, 2019, **31**, 1902709.

56. J.-T. Ren, L. Chen, H.-Y. Wang and Z.-Y. Yuan, *ACS Appl. Mater. Interfaces*, 2021, **13**, 12106-12117.

57. D. Wu, H. Wang, H. Huang, R. Zhang, L. Ji, H. Chen, Y. Luo, J. You, D. Tang and Z. Zhang, *Chem. Commun.*, 2019, **55**, 7546-7549.

58. N. Cao, Z. Chen, K. Zang, J. Xu, J. Zhong, J. Luo, X. Xu and G. Zheng, *Nat. Commun.*, 2019, **10**, 1-12.

59. J.-T. Ren, L. Chen, Y. Liu and Z.-Y. Yuan, *J. Mater. Chem. A*, 2021, **9**, 11370-11380.

60. M.-C. Kim, H. Nam, J. Choi, H. S. Kim, H. W. Lee, D. Kim, J. Kong, S. S. Han, S. Y. Lee and H. S. Park, *ACS Catal.*, 2020, **10**, 10577-10584.

61. A. Liu, X. Liang, Q. Yang, X. Ren, M. Gao, Y. Yang and T. Ma, *ChemElectroChem*, 2020, **7**, 4900-4905.

62. L. Li, C. Tang, D. Yao, Y. Zheng and S.-Z. Qiao, *ACS Energy Lett.*, 2019, **4**, 2111-2116.